Nuclear Instruments and Methods in Physics Research A307 (1991) 398–412
North-Holland

Calculated neutron response of a Bonner sphere spectrometer with ^{3}He counter

Vladimir Mares [1], Gertraude Schraube and Hans Schraube

GSF – Forschungszentrum für Umwelt und Gesundheit, GmbH, Institut für Strahlenschutz, Auswertungsstelle für Strahlendosimeter, D-8042 Neuherberg, Germany

Received 11 February 1991 and in revised form 3 June 1991

The neutron response matrix for a Bonner sphere spectrometric system with a 3.2 cm diameter ^{3}He proportional counter is calculated applying the MCNP Monte Carlo code. The effects of variations in density of the polyethylene moderators and in gas pressure of the ^{3}He counter are also discussed.

1. Introduction

The use of the Bonner sphere spectrometer (BSS) based on spherical polyethylene moderators is a nearly universal method of neutron detection for radiological protection purposes. A BSS consists of a detector for thermal neutrons situated in the center of various polyethylene spheres with diameters between approximately 2 in. (5.08 cm) and 18 in. (45.72 cm). The active thermal neutron detectors can be scintillators (^{6}LiI(Eu)) combined with a photomultiplier or proportional counters filled with $^{10}BF_3$ or ^{3}He gas.

The main advantages of the BSS are the very wide energy range of detection from thermal to tens of MeV, and the isotropic response resulting from the spherically symmetric shape of the moderators.

Since 1960, when the BSS was first introduced by Bramblett, Ewing and Bonner [1] a number of studies on its energy or integral response have been performed (see, e.g. refs. [2–10]). Furthermore, the responses have been studied for some variations in type and size of the thermal neutron detector [4,8]. Any kind of unfolding procedure for the determination of the energy distribution [11–13], or linear combination method for direct determination of integral parameters [3,6,7,11] requires an exact knowledge of the response matrix. Depending on the type of unfolding, any intrinsic error of the data matrix may produce unacceptable errors in the resulting neutron fluence distribution.

The effect of an inappropriate choice of response matrix on unfolded neutron spectra has been clearly shown by Lowry and Johnson [9]. The results of this study emphasized the need for further calculations and experimental verification of the Bonner sphere response matrix.

While for many years measurements and calculations were made for ^{6}LiI(Eu) based systems, in the seventies small cylindrical ^{3}He filled proportional counters became available [14] which, however, had some operational problems. Recently, larger spherical ^{3}He proportional detectors were used [15] which provide high sensitivity combined with good discrimination against photon background and electronic noise with good long term operational characteristics. The required data of the response matrix for this size and type of thermal neutron detector, however, are not yet available.

There are two approaches to determine the BSS response matrix: experimental calibration in monoenergetic neutron fields and neutron transport calculations.

The experiments are limited by five factors: i) the relatively small number of available monoenergetic neutron fields under calibration field conditions [15,16], ii) the limited energy range where neutron fields may be generated at all, iii) the room and air scattering of neutrons which disturbs the direct neutron component, iv) geometrical effects [17,18], and v) in part the poor counting statistics, especially in energy ranges where the response of the actual sphere is low, or the respective neutron source is weak.

The accuracy of the calculations depends on the method of solving the radiation transport problem, on the accuracy of the cross section data, on the possible energy binning, on the precision of the geometrical

[1] On leave from Technical University Prague, Czechoslovakia.

Elsevier Science Publishers B.V.

modelling and on the influence of variance reducing methods. Although recently powerful computer systems became available which allow a predefined calculational precision to be achieved within an acceptable computer time, it is generally difficult to define any trustworthy figure for the accuracy.

The aim of this study is to provide a reliable response matrix for a Bonner sphere spectrometer equipped with a 3.2 cm diameter ^{3}He proportional counter, by means of Monte Carlo calculations.

2. Geometrical and physical definitions

The Monte Carlo calculations of the BSS response were performed for a commercially available ^{3}He spherical proportional counter with a diameter of 3.2 cm, placed in the center of polyethylene moderating spheres with different diameters in the range from 2 to 15 in.. For historical reasons and for comparison with other published results, the choice of the sphere diameters was retained to be integer values in units of inch. For diameters smaller than 5 in., steps of $\frac{1}{2}$ in. were used. It should be stressed, however, that the specific size of the thermal neutron counter occupies a relatively large volume, reducing the effective moderator thickness compared to systems with less voluminous counters. Consequently, it is expected that the energy dependence of response will differ when different counter volumes are used. The effect will be highest at the smallest BS-diameters.

Table 1 shows the diameters of the spheres considered together with the respective polyethylene shell thicknesses.

For the calculations it was assumed that the counter fits into the moderator without any air gap. The material of the counter wall was neglected as well as the duct for the counter cable.

Table 1
Relation between Bonner sphere diameter d and thickness of the polyethylene shell for two counter diameters

Sphere diameter d		Shell thickness [cm] for counter diameter	
[in.]	[cm]	3.2 cm	1.0 cm
2.0	5.08	0.94	2.04
2.5	6.35	1.58	2.68
3.0	7.62	2.21	3.31
3.5	8.89	2.85	3.95
4.0	10.16	3.48	4.58
4.5	11.43	4.12	5.22
5.0	12.70	4.75	5.85
6.0	15.24	6.02	7.12
7.0	17.78	7.29	8.39
8.0	20.32	8.56	9.66
10.0	25.40	11.10	12.20
12.0	30.48	13.64	14.74
15.0	38.10	17.45	18.55

The gas filling was assumed to be of 172 kPa, which was the pressure adopted during a comparative benchmark study, initiated by the European Dosimetry group EURADOS-CENDOS, and which is close to experimentally determined values [19]. Any additional krypton gas filling (in the benchmark study 100 kPa Kr) was not taken into account, because cross section data were not available in the input format suitable for the neutron transport code used in the calculations. It was assumed, however, that the probability for any nuclear reaction of neutrons with Kr is negligible compared with the ^{3}He(n, p) reactions.

The helium number density related to the specified partial pressure was calculated to be $n(^3\text{He}) = 4.2497 \times 10^{19}$ cm^{-3} at 293 K. The density of the spherical polyethylene moderators was assumed to be $\rho = 0.95$ g cm^{-3}.

The response of the BSS to neutrons was calculated for broad parallel beam geometry for 27 values of neutron energy in the range from 1.0×10^{-8} to 30 MeV. The discrete neutron energy values were selected on the following basis: firstly, 11 out of the 14 reference energies given by ISO [20] were used to agree with conditions which may be realized experimentally. Secondly, additional energy points at logarithmic equidistant intervals and at decade boundaries were selected. Finally, 30 MeV was added as the upper limit of the calculations, although it was recognized that the data basis for this energy may be weak.

3. Calculational procedures

3.1. Choice of the transport code

Three program packages were under consideration for the solution of the radiation transport problem, whose features will be described here briefly: i) The one dimensional discrete ordinate transport code ANISN, ii) the Monte Carlo code SAM-CE, and iii) the Monte Carlo code MCNP. The latter was the code actually applied.

3.1.1. The ANISN Code

The adjoint technique of Hansen and Sandmeier [21] has been widely used for the calculation of Bonner sphere responses [4,8,10] applying the one dimensional discrete ordinate transport code ANISN [22].

This method is the most common deterministic method which solves the transport equation for the average particle behavior. Furthermore, the adjoint flux technique allows the response of each Bonner sphere to be obtained in one computational run rather

than by performing the forward computation for each respective neutron energy. The technique assumes that the adjoint source is distributed throughout the detector volume and the detection system is placed in a parallel beam of neutrons. This results in a continuous neutron fluence distribution, which represents the energy response, for e.g. thermal neutrons in the detector.

One of the most recent works [10] on the response matrix for a Bonner sphere system equipped with a small ^{3}He cylindrical counter with 9 mm × 9 mm diameter sensitive volume [14], 80 kPa ^{3}He and 20 kPa Kr gas filling was performed using the ANISN code.

In contrast to the discrete ordinate transport code, Monte Carlo codes do not solve an explicit equation, but rather duplicate the statistical process and are useful for complex problem that cannot be modelled by deterministic methods.

3.1.2. The SAM-CE Monte Carlo Code

SAM-CE is a Monte Carlo code [23] designed to solve time-dependent neutron and gamma ray transport problems in three-dimensional geometries. It is applicable for forward neutron and electron calculations and for forward as well as adjoint primary gamma ray calculations and can be used for both fixed source and eigenvalue calculations. All neutron and gamma ray cross-section data are taken from the ENDF libraries and are tabulated in point energy meshes. The code contains a thermal neutron cross-section treatment and thermal neutron diffusion options. For low energy neutron problems, however, it cannot be recommended because of the absence of S(alpha, beta) tables for polyethylene in a format suitable to SAM-CE. These tables are required to enable a complete representation of thermal neutron scattering by molecules at room temperature for neutron energies less than 4 eV. Furthermore, the code is no longer updated; the last version of SAM-CE distributed through the Radiation Shielding Information Center (RSIC) at Oak Ridge National Laboratory by the NEA Data Bank at Sacley in France is from 1979.

3.1.3. The MCNP Monte Carlo Code

The Monte Carlo code used in the present calculations was the MCNP code version 3B3 [24,25] distributed through RSIC by the NEA Data Bank. It represents the most extensive Monte Carlo program that is available in the public domain and is continually updated to take advantage of advances in computer hardware and software.

3.2. Calculation input and parameters

The MCNP code which is written in Fortran 77 was implemented to run under the UNIX operation system on the GSF CONVEX C220S computer, which is a very fast parallel super computer with vector architecture.

The MCNP cross-section treatment is continuous in energy with linear interpolation between specific energies so that the original data are reproduced in most cases to within 0.5%. All reaction types from the basic data are included for neutron energies from 10^{-5} eV to 20 MeV and for gamma rays from 1 keV to 100 MeV. Between 20 and 30 keV neutron energy, the code extrapolates the available cross section data.

The MCNP cross-section data distributed by RSIC are generated by running the NJOY nuclear data processing systems [26] to extract evaluated data from many sources such as the ENDF/B-III, -IV, -V [27], the ENDL-73, -75, -76, -79, -85 [28], and the LASL-SUB (the latter is the Los Alamos Sublibrary which is a collection of special data evaluated at the Los Alamos Laboratories), among others.

The continuous-energy neutron cross-section data of elements used for the calculations presented in this article were extracted from the following sources: hydrogen from ENDF/B-IV Rev. 1, ^{3}He from ENDF/B-III and carbon from LASL-SUB 1976. The thermal S(alpha, beta) tables for polyethylene were taken from a special set of ENDF tapes [29]. The cross-section data were previously generated in a suitable format to be used as an input of the MCNP by the NJOY nuclear data processing system, and were available in the standard MCNP package.

The geometry treatment of MCNP allows three-dimensional configurations to be defined in a Cartesian coordinate system. Volumes, which can contain specified materials, are built up by using Boolean operators to combine basic geometric cells bounded by first- and second-degree surfaces.

The MCNP tracks particles through the geometry by sampling possible random walks and assigns a score of user-specified quantities. Standard MCNP tallies are normalised to one starting particle. The output contains also the relative error $R = s_{\bar{x}}/\bar{x}$ of the mean value $\bar{x}$ of the scored quantity, averaged over the N results of N histories in the problem.

In order to avoid additional sources of systematic errors, only minimal use was made of variance reducing methods. In the present calculations, the geometry splitting and the Russian roulette technique were introduced, which enhance or reduce the number of additional histories, with appropriate weights at the boundaries of the geometrical cells.

The modelling of the broad parallel beam geometry was performed in the following way: The positions of the starting particles were sampled uniformly on the surface of a disk source which is centered on and perpendicular to an axis of the sphere. All neutron tracks were parallel to the source–detector axis, and

fully included the whole surface of the moderating sphere (fig. 1). The space between source and Bonner sphere was assumed to be vacuum.

The standard MCNP code can only solve the forward transport equation. Although there is a multigroup patch for MCNP called MCMG with both forward and adjoint modes of operation, this was not available in the standard MCNP package.

4. Results and discussion

4.1. Pressure dependence of response

As a first step, calculations of the responses were performed for different counter gas pressures for several Bonner spheres and neutron energies.

Fig. 2 shows as an example the dependence of response on the pressure for the 4 in. and 6 in. spheres, for neutron energies of 10 eV and 14.8 MeV, normalised to the standard pressure ($p_0 = 172$ kPa) condition. Cubic polynomials are fitted through the data points with a maximum uncertainty of $\pm 2\%$. It can be seen that an increase of the pressure by 20%, results in a 10% increase compared with the response at the standard pressure. At higher pressures the increase of the response starts to depend on sphere diameter and neutron energy. A reduction of the pressure by the same amount reduces the response by 12% for the four conditions under consideration.

4.2. Energy dependence of response

The response of the BSS was calculated as the number of counts per incident neutron fluence. The resulting numerical values of the energy response of the Bonner multisphere set for the spheres from 2 in. to 15 in. diameter and the bare proportional counter at the 27 energy points are given in table 2, together with

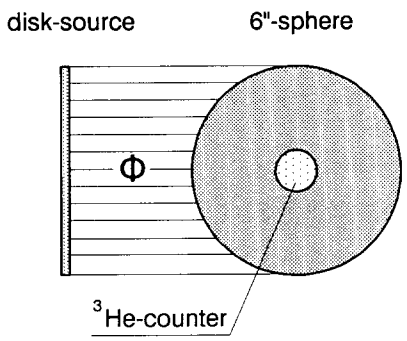

Fig. 1. General view of the geometric setup simulated in the calculations. Φ is the incoming neutron fluence to which the response is related.

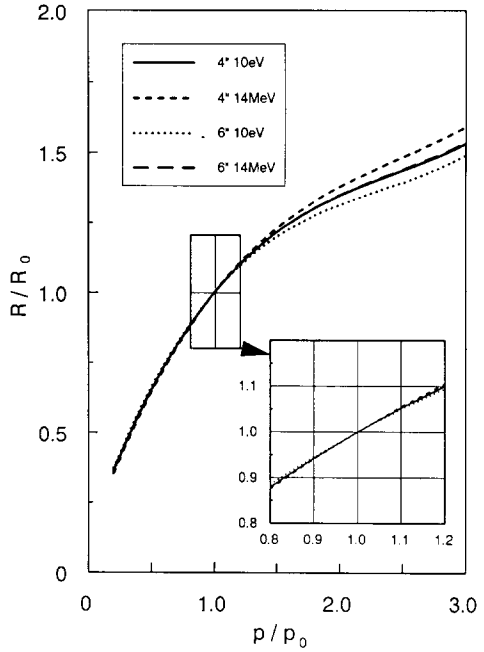

Fig. 2. Dependence of the response ratio R/R_0 on the gas pressure p normalised to the standard pressure conditions ($p_0 = 172$ kPa). The data points, which fit the curves within $\pm 2\%$ are omitted for clarity.

the standard error of the mean. The standard error of the mean derives only from the Monte Carlo statistics and includes no contribution from uncertainties in the modelling, the cross sections etc.

Fig. 3 shows as an example the responses for the discrete monoenergetic neutrons as a function of the sphere diameter. It can be seen that the maximum of the responses is shifting towards higher sphere diameters with increasing neutron energy. This reflects the physical effect that with increasing neutron energy the maximum of the thermal neutron fluence rate migrates deeper into the moderator. This general behaviour is known from the literature. The differences between these and the present results will be discussed in section 4.6.

4.3. Semi-empirical representation of the responses

On the basis of physical and mathematical considerations, Zaborowski [30] suggested that the response versus the sphere diameter could be represented by a log–normal distribution:

$$R(d_i, E) = \frac{P_1(E)}{P_2(E) d_i} \exp\left(- \frac{(\ln d_i - P_3(E))^2}{2 P_2^2(E)} \right), \quad (1)$$

where d_i are the sphere diameters in cm, E is the neutron energy and P_1, P_2, P_3 three parameters to be determined.

The above semi-empirical representation was used for a cross check. A typical example is given in fig. 4 for three arbitrarily chosen energies. It is observed that this representation does fit the present data well; however, it should be stressed that for neutron energies below 1 eV this is generally not the case.

The parameters $P_{1,2,3}$ of the response function $R(d_i, E)$ were calculated for 27 discrete values of neutron energy to fit the MCNP calculated responses. The data for the parameters are listed in table 3. Additionally, the energy dependence of the parameters is shown in fig. 5, which exhibit surprisingly smooth characteristics. From these data it is possible, using the function $R(d_i, E)$, to obtain a reasonable first estimate for the response of any Bonner sphere at any discrete neutron energy.

4.4. Effect of polyethylene density

The density of commercial polyethylene ranges between 0.91 and 0.97 g cm^{-3}. In a first approximation, the effect of increasing density is comparable to an increase of the sphere diameter. The most commonly used polyethylene has a density of 0.95 g cm^{-3} and this was the value assumed in the present calculations. In fig. 6 the responses of Bonner spheres calculated for three different polyethylene densities (0.92, 0.95, 1.0 g cm^{-3}) are shown for four particular neutron energies.

The following effects were observed: by increasing the polyethylene density from 0.95 to 1.00 g cm^{-3}, the characteristic shape of the response becomes narrower and the maximum shifts to smaller sphere diameters. Decreasing the density from 0.95 to 0.92 g cm^{-3} has the inverse effect. For 1.2 MeV the differences in response were up to 16%, for densities of 0.95 and 0.92 g cm^{-3}, respectively; for 0.316 eV the differences were approximately up to 24%. Generally, increasing the polyethylene density results in decreasing the responses at the lower energies and increasing it at higher energies.

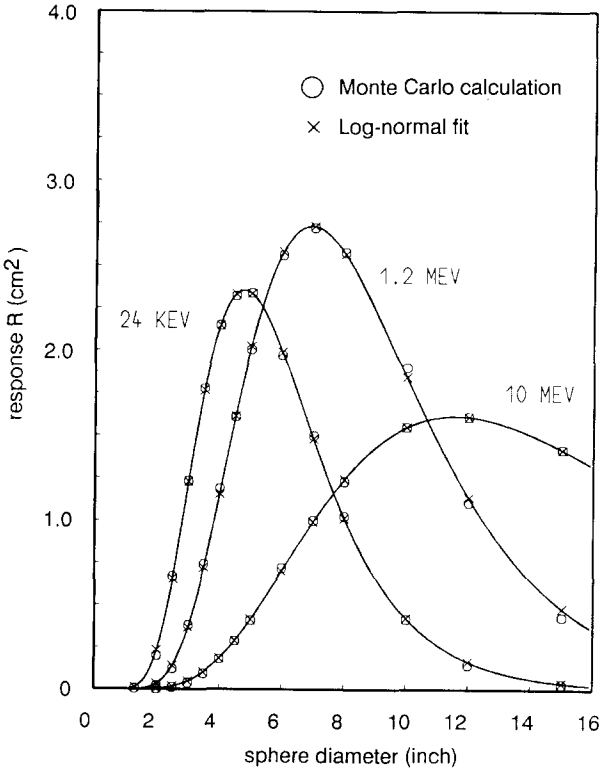

Fig. 4. Log–normal representation of the BSS-responses shown for 24 keV, 1.2 MeV and 10 MeV neutron energy.

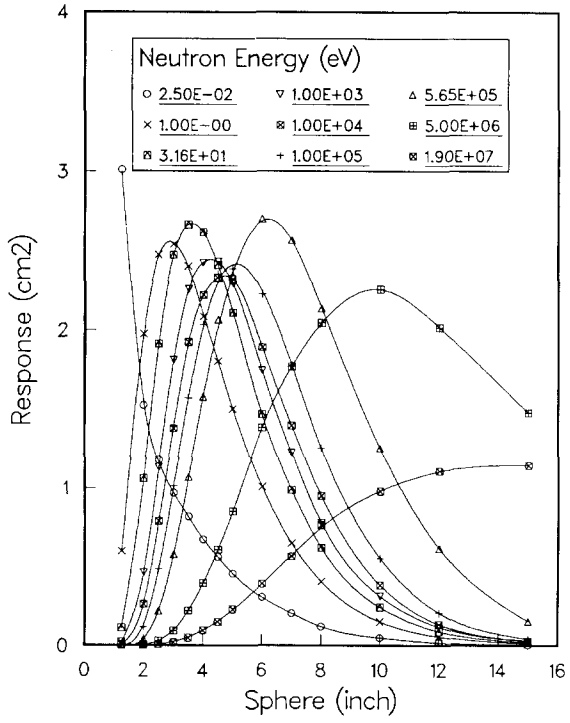

Fig. 3. Neutron responses of the Bonner sphere system with ^{3}He counter as a function of the sphere diameter, as calculated by the MCNP code.

4.5. Interpolation of the responses

The response data obtained from MCNP calculations were then interpolated to generate a response matrix having 49 energy points in log-equidistant intervals (i.e. 5 per decade) from 0.01 eV to 30 MeV, for spheres with a diameter of 2–15 in., in steps of 0.5 in. The responses for the additional Bonner spheres were

Table 2
Numerical values of the calculated responses R (cm^2) of the bare ^3He counter and the 13 Bonner spheres at the 27 neutron energies. Each value is followed by a two digit number which indicates the estimated standard error of the mean in percent

Number	E [ev]	Bare	2 in.	2.5 in.	3 in.	3.5 in.	4 in.	4.5 in.
1	1.000E − 02	4.162E + 00 0.4	1.240E + 00 0.6	9.384E − 01 0.8	7.938E − 01 1.1	6.642E − 01 1.6	5.491E − 01 1.4	4.576E − 01 1.7
2	2.500E − 02	3.012E + 00 0.4	1.515E + 00 0.5	1.181E + 00 0.7	9.702E − 01 0.9	8.185E − 01 1.0	6.735E − 01 1.0	5.611E − 01 1.6
3	1.000E − 01	1.719E + 00 0.3	2.004E + 00 0.4	1.817E + 00 0.6	1.593E + 00 0.8	1.367E + 00 0.8	1.134E + 00 1.0	9.287E − 01 1.2
4	3.160E − 01	1.023E + 00 0.3	2.148E + 00 0.4	2.337E + 00 0.5	2.211E + 00 0.9	1.977E + 00 0.7	1.663E + 00 0.8	1.417E + 00 1.0
5	1.000E + 00	5.978E − 01 0.3	1.975E + 00 0.4	2.477E + 00 0.5	2.542E + 00 0.6	2.403E + 00 0.6	2.087E + 00 0.7	1.803E + 00 0.9
6	3.160E + 00	3.418E − 01 0.3	1.672E + 00 0.4	2.387E + 00 0.5	2.678E + 00 0.8	2.638E + 00 0.6	2.398E + 00 0.7	2.069E + 00 0.9
7	1.000E + 01	1.941E − 01 0.3	1.359E + 00 0.5	2.193E + 00 0.5	2.635E + 00 0.5	2.728E + 00 0.6	2.603E + 00 0.6	2.316E + 00 0.8
8	3.160E + 01	1.102E − 01 0.3	1.063E + 00 0.5	1.912E + 00 0.5	2.473E + 00 0.9	2.664E + 00 0.6	2.617E + 00 0.7	2.412E + 00 0.8
9	1.000E + 02	6.237E − 02 0.3	8.108E − 01 0.6	1.629E + 00 0.6	2.227E + 00 0.7	2.553E + 00 0.6	2.585E + 00 0.7	2.427E + 00 0.8
10	3.160E + 02	3.535E − 02 0.3	6.162E − 01 0.7	1.354E + 00 0.6	2.010E + 00 1.0	2.404E + 00 0.6	2.533E + 00 0.7	2.472E + 00 0.8
11	1.000E + 03	2.031E − 02 0.3	4.618E − 01 0.8	1.133E + 00 0.7	1.811E + 00 0.7	2.260E + 00 0.6	2.425E + 00 0.7	2.431E + 00 0.8
12	2.000E + 03	1.450E − 02 0.3	3.913E − 01 0.9	1.019E + 00 0.7	1.652E + 00 1.1	2.146E + 00 0.6	2.374E + 00 0.7	2.428E + 00 0.8
13	3.160E + 03	1.131E − 02 0.3	3.427E − 01 0.9	9.536E − 01 0.7	1.578E + 00 1.1	2.083E + 00 0.6	2.349E + 00 0.7	2.376E + 00 0.8
14	1.000E + 04	6.261E − 03 0.3	2.601E − 01 1.1	7.898E − 01 0.8	1.378E + 00 0.8	1.923E + 00 0.7	2.224E + 00 0.7	2.328E + 00 0.8
15	2.400E + 04	4.169E − 03 0.3	2.007E − 01 1.2	6.701E − 01 0.9	1.230E + 00 1.3	1.776E + 00 0.8	2.150E + 00 0.9	2.323E + 00 0.9
16	3.160E + 04	3.721E − 03 0.3	1.848E − 01 1.3	6.382E − 01 0.9	1.224E + 00 1.0	1.744E + 00 0.8	2.123E + 00 0.9	2.324E + 00 0.9
17	1.000E + 05	2.680E − 03 0.3	1.176E − 01 1.6	4.837E − 01 1.1	1.017E + 00 1.1	1.569E + 00 0.9	2.033E + 00 0.9	2.354E + 00 0.9
18	1.440E + 05	2.478E − 03 0.3	9.924E − 02 1.7	4.323E − 01 1.1	9.349E − 01 1.5	1.500E + 00 0.9	1.985E + 00 0.9	2.280E + 00 1.0
19	2.500E + 05	2.272E − 03 0.3	7.130E − 02 2.0	3.448E − 01 1.3	8.218E − 01 1.6	1.346E + 00 0.9	1.875E + 00 0.9	2.254E + 00 1.0
20	5.650E + 05	2.039E − 03 0.3	3.773E − 02 2.7	2.178E − 01 1.6	5.766E − 01 1.9	1.071E + 00 1.1	1.578E + 00 1.0	2.065E + 00 1.0
21	1.200E + 06	2.191E − 03 0.3	2.096E − 02 2.8	1.209E − 01 1.6	3.823E − 01 1.5	7.433E − 01 1.3	1.186E + 00 1.2	1.608E + 00 1.1
22	2.500E + 06	2.257E − 03 0.3	1.025E − 02 2.7	6.041E − 02 1.7	1.957E − 01 1.8	4.217E − 01 1.7	7.227E − 01 1.4	1.069E + 00 1.0
23	5.000E + 06	1.753E − 03 0.3	5.220E − 03 3.6	2.799E − 02 2.5	9.216E − 02 2.9	2.191E − 01 2.4	3.946E − 01 2.0	6.075E − 01 1.8
24	1.000E + 07	1.133E − 03 0.3	2.297E − 03 4.0	1.151E − 02 3.8	3.795E − 02 3.4	9.523E − 02 2.8	1.813E − 01 2.3	2.871E − 01 2.0
25	1.480E + 07	8.207E − 04 0.3	1.647E − 03 4.1	7.682E − 03 4.5	2.643E − 02 5.0	6.677E − 02 3.0	1.225E − 01 3.3	2.124E − 01 2.2
26	1.900E + 07	6.523E − 04 0.3	1.253E − 03 5.0	5.608E − 03 4.2	1.915E − 02 4.3	4.762E − 02 3.3	9.494E − 02 3.1	1.476E − 01 2.3
27	3.000E + 07	6.216E − 04 0.3	8.569E − 04 4.6	2.978E − 03 4.7	8.591E − 03 4.4	2.239E − 02 4.6	4.307E − 02 4.3	7.842E − 02 3.6

Table 2 (continued)

Number	E [eV]	5 in.	6 in.	7 in.	8 in.	10 in.	12 in.	15 in.
1	1.000E − 02	3.742E − 01 1.8	2.396E − 01 2.6	1.616E − 01 2.6	9.358E − 02 3.7	3.735E − 02 3.8	1.196E − 02 4.5	2.811E − 03 4.6
2	2.500E − 02	4.545E − 01 1.7	3.045E − 01 1.9	2.021E − 01 2.5	1.191E − 01 3.3	4.844E − 02 3.6	1.724E − 02 4.1	3.816E − 03 4.8
3	1.000E − 01	7.549E − 01 1.3	5.011E − 01 1.8	3.248E − 01 1.9	2.049E − 01 2.5	7.976E − 02 2.8	2.760E − 02 4.7	6.099E − 03 4.2
4	3.160E − 01	1.173E + 00 1.1	7.814E − 01 1.5	4.829E − 01 1.5	3.090E − 01 2.1	1.153E − 01 2.3	4.277E − 02 3.7	9.453E − 03 4.4
5	1.000E + 00	1.502E + 00 0.9	1.010E + 00 1.4	6.484E − 01 1.3	4.039E − 01 1.9	1.490E − 01 2.0	5.553E − 02 3.2	1.117E − 02 4.7
6	3.160E + 00	1.756E + 00 0.9	1.185E + 00 1.2	7.565E − 01 1.2	4.737E − 01 1.7	1.808E − 01 1.9	6.649E − 02 2.9	1.500E − 02 4.5
7	1.000E + 01	1.976E + 00 0.8	1.391E + 00 1.0	9.030E − 01 1.4	5.654E − 01 1.7	2.098E − 01 1.7	7.198E − 02 2.7	1.714E − 02 3.5
8	3.160E + 01	2.112E + 00 0.8	1.468E + 00 1.1	9.888E − 01 1.1	6.194E − 01 1.6	2.414E − 01 1.6	8.814E − 02 2.6	1.810E − 02 4.0
9	1.000E + 02	2.194E + 00 0.8	1.603E + 00 1.1	1.043E + 00 1.1	6.763E − 01 1.5	2.631E − 01 1.6	9.467E − 02 2.6	2.085E − 02 3.8
10	3.160E + 02	2.253E + 00 0.8	1.639E + 00 1.1	1.135E + 00 1.1	7.437E − 01 1.5	2.844E − 01 1.5	1.058E − 01 2.4	2.196E − 02 3.8
11	1.000E + 03	2.294E + 00 0.8	1.744E + 00 1.1	1.224E + 00 1.0	7.804E − 01 1.4	3.109E − 01 1.5	1.170E − 01 2.3	2.460E − 02 3.9
12	2.000E + 03	2.321E + 00 0.8	1.807E + 00 1.1	1.262E + 00 1.0	8.273E − 01 1.4	3.234E − 01 1.5	1.259E − 01 2.3	2.571E − 02 3.9
13	3.160E + 03	2.318E + 00 0.8	1.832E + 00 1.1	1.272E + 00 1.0	8.675E − 01 1.4	3.322E − 01 1.5	1.239E − 01 2.2	2.695E − 02 4.8
14	1.000E + 04	2.321E + 00 0.8	1.891E + 00 1.1	1.396E + 00 1.0	9.515E − 01 1.4	3.819E − 01 1.4	1.330E − 01 2.1	2.938E − 02 3.9
15	2.400E + 04	2.339E + 00 0.8	1.972E + 00 1.0	1.497E + 00 1.2	1.025E + 00 1.6	4.173E − 01 1.6	1.443E − 01 2.9	3.229E − 02 3.1
16	3.160E + 04	2.311E + 00 0.8	2.010E + 00 1.0	1.544E + 00 1.2	1.034E + 00 1.6	4.347E − 01 1.6	1.566E − 01 2.8	3.558E − 02 3.0
17	1.000E + 05	2.387E + 00 0.8	2.230E + 00 1.0	1.778E + 00 1.1	1.253E + 00 1.5	5.529E − 01 1.5	2.054E − 01 2.5	4.133E − 02 4.1
18	1.440E + 05	2.441E + 00 0.8	2.316E + 00 1.0	1.943E 00 1.1	1.384E + 00 1.4	6.238E − 01 1.4	2.403E − 01 3.1	4.845E − 02 4.7
19	2.500E + 05	2.472E + 00 0.8	2.543E + 00 0.9	2.196E + 00 1.0	1.633E + 00 1.3	7.842E − 01 1.3	3.276E − 01 2.1	7.826E − 02 5.0
20	5.650E + 05	2.347E + 00 0.8	2.701E + 00 0.9	2.568E + 00 1.0	2.139E + 00 1.2	1.253E + 00 1.0	6.160E − 01 1.6	1.526E − 01 4.5
21	1.200E + 06	2.003E + 00 1.1	2.562E + 00 1.1	2.724E + 00 1.3	2.578E + 00 1.3	1.899E + 00 1.6	1.107E + 00 1.8	4.315E − 01 4.6
22	2.500E + 06	1.410E + 00 1.3	1.995E + 00 1.2	2.353E + 00 1.3	2.512E + 00 1.4	2.307E + 00 1.8	1.779E + 00 2.5	9.975E − 01 3.7
23	5.000E + 06	8.521E − 01 1.7	1.383E + 00 1.6	1.769E + 00 1.6	2.045E + 00 1.4	2.258E + 00 1.1	2.016E + 00 1.4	1.478E + 00 2.0
24	1.000E + 07	4.103E − 01 1.8	7.204E − 01 1.6	9.981E − 01 2.1	1.228E + 00 1.6	1.547E + 00 1.3	1.609E + 00 1.5	1.417E + 00 3.2
25	1.480E + 07	2.963E − 01 2.0	5.202E − 01 2.4	7.389E − 01 2.3	9.242E − 01 2.3	1.208E + 00 2.5	1.335E + 00 2.9	1.305E + 00 3.2
26	1.900E + 07	2.268E − 01 2.1	3.898E − 01 1.9	5.641E − 01 2.7	7.642E − 01 2.2	9.804E − 01 1.7	1.110E + 00 1.8	1.146E + 00 2.6
27	3.000E + 07	1.199E − 01 3.2	2.313E − 01 2.8	3.397E − 01 3.5	4.463E − 01 3.0	6.305E − 01 2.2	7.689E − 01 2.4	8.449E − 01 3.6

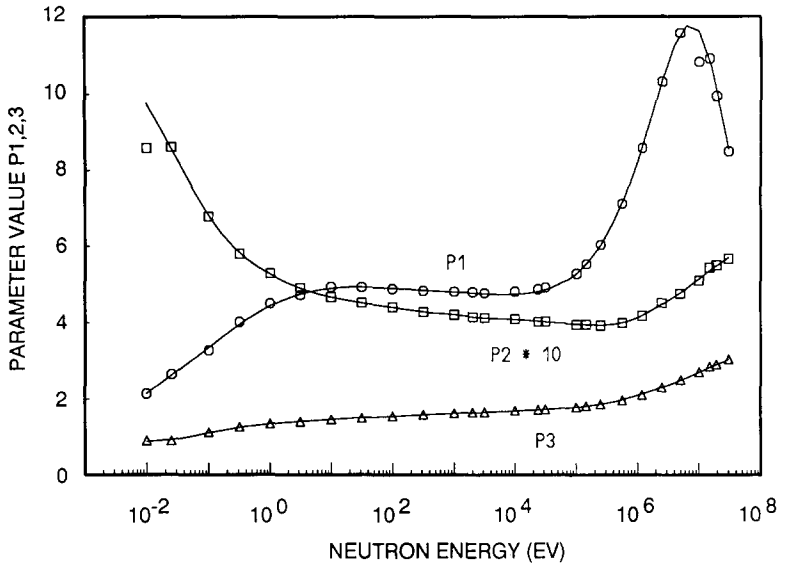

Fig. 5. Parameters of log–normal representation of the BSS-responses versus the neutron energy (P_2 has been multiplied by a factor of 10).

Table 3
Parameters P_1, P_2, and P_3 of eq. (1) for the best fit of the calculated response R versus the sphere diameter d, for the 27 neutron energies E

E [eV]	P_1	P_2	P_3
1.00E−02	2.1345	0.8578	0.8972
2.50E−02	2.6452	0.8605	0.8938
1.00E−01	3.2794	0.6782	1.1206
3.16E−01	4.0166	0.5803	1.2595
1.00E−00	4.4957	0.5287	1.3443
3.16E−00	4.7269	0.4900	1.4009
1.00E+01	4.9351	0.4669	1.4590
3.16E+01	4.9258	0.4520	1.5022
1.00E+02	4.8861	0.4403	1.5455
3.16E+02	4.8331	0.4278	1.5822
1.00E+03	4.8060	0.4203	1.6183
2.00E+03	4.7991	0.4145	1.6409
3.16E+03	4.7773	0.4124	1.6528
1.00E+04	4.8155	0.4090	1.6910
2.40E+04	4.8743	0.4020	1.7194
3.16E+04	4.9179	0.4029	1.7284
1.00E+05	5.2791	0.3946	1.7802
1.44E+05	5.5298	0.3950	1.8097
2.50E+05	6.0325	0.3921	1.8578
5.65E+05	7.1065	0.3991	1.9627
1.20E+06	8.5790	0.4167	2.1060
2.50E+06	10.3179	0.4512	2.3052
5.00E+06	11.5814	0.4756	2.4974
1.00E+07	10.8282	0.5097	2.7083
1.48E+07	10.9232	0.5434	2.8471
1.90E+07	9.9513	0.5498	2.9043
3.00E+07	8.4908	0.5669	3.0412

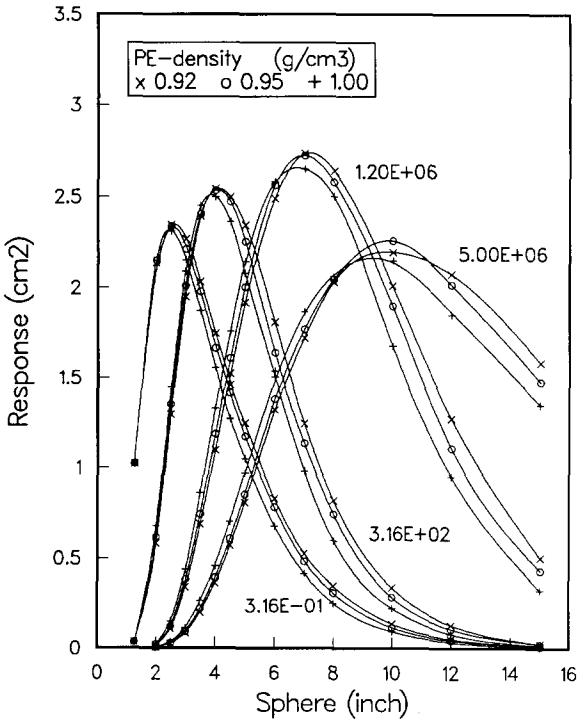

Fig. 6. Variations of response with the polyethylene density for 0.316 eV, 316 eV, 1.2 MeV and 5 MeV.

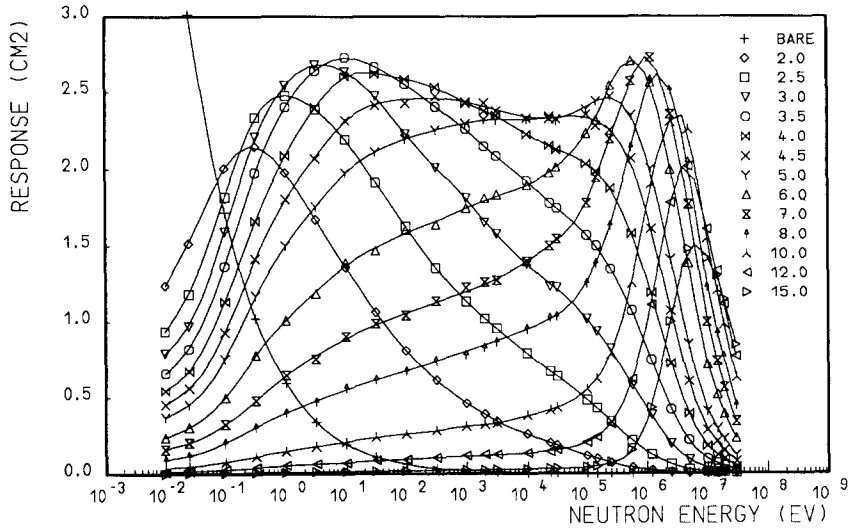

Fig. 7. Energy response of BSS, as calculated with MCNP (data points). The lines connect the responses of the 49 energies of the final matrix.

interpolated in the sphere diameter domain (fig. 3) for each respective neutron energy using the cubic spline interpolation method which smooths out the estimated statistical uncertainties. The same method was then used for the interpolation in the (logarithmic) energy domain for all response data obtained both from MCNP calculation and from the sphere diameter interpolation.

Fig. 7 shows the original 27 MCNP calculated responses (points) and the interpolated response matrix data (curve) for the Bonner spheres versus neutron energy. (The 49 interpolated data points are omitted for charity.) It is obvious that the interpolated response matrix data represent the MCNP calculated responses very well. The differences are usually less than 1%, only in 16% of cases were the differences larger, but they never exceed 4.5%.

Similarly in fig. 8, responses interpolated in the sphere diameter domain for sphere diameters which were not explicitly calculated by the MNCP code are

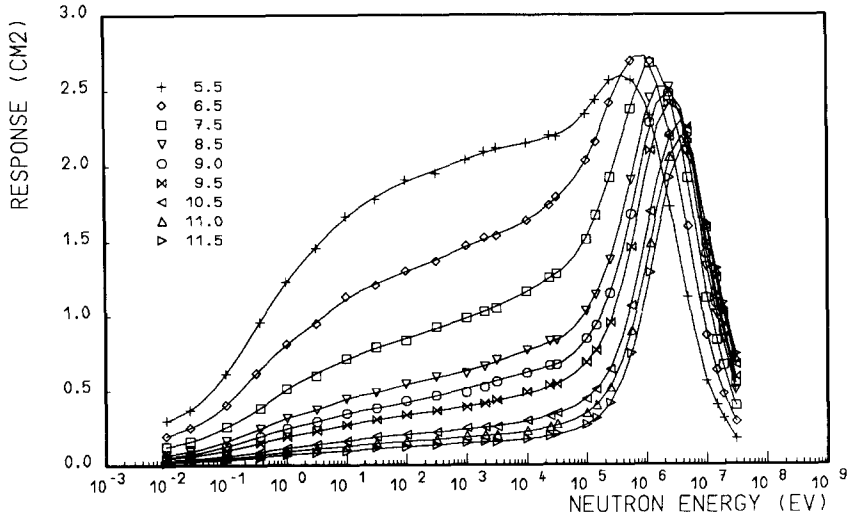

Fig. 8. Energy response of BSS for spheres interpolated in the sphere diameter domain (data points). The lines have the same meaning as in fig. 7.

Table 4
Response matrix of the Bonner sphere spectrometer interpolated at 49 log equidistant neutron energies and 22 spheres

Number	E [eV]	Bare	2 in.	2.5 in.	3 in.	3.5 in.	4 in.	4.5 in.	5 in.
1	1.000E−02	4.150E+00	1.239E+00	9.366E−01	7.907E−01	6.605E−01	5.474E−01	4.564E−01	3.735E−01
2	1.585E−02	3.565E+00	1.372E+00	1.048E+00	8.674E−01	7.283E−01	6.002E−01	5.020E−01	4.082E−01
3	2.512E−02	3.013E+00	1.520E+00	1.186E+00	9.763E−01	8.227E−01	6.762E−01	5.634E−01	4.559E−01
4	3.981E−02	2.521E+00	1.688E+00	1.369E+00	1.141E+00	9.641E−01	7.934E−01	6.537E−01	5.277E−01
5	6.310E−02	2.090E+00	1.857E+00	1.585E+00	1.353E+00	1.149E+00	9.492E−01	7.765E−01	6.276E−01
6	1.000E−01	1.719E+00	2.002E+00	1.819E+00	1.595E+00	1.370E+00	1.136E+00	9.325E−01	7.579E−01
7	1.585E−01	1.403E+00	2.100E+00	2.050E+00	1.848E+00	1.613E+00	1.344E+00	1.119E+00	9.169E−01
8	2.512E−01	1.137E+00	2.145E+00	2.250E+00	2.088E+00	1.857E+00	1.557E+00	1.316E+00	1.086E+00
9	3.981E−01	9.192E−01	2.133E+00	2.389E+00	2.286E+00	2.075E+00	1.755E+00	1.501E+00	1.244E+00
10	6.310E−01	7.420E−01	2.071E+00	2.460E+00	2.436E+00	2.256E+00	1.931E+00	1.662E+00	1.381E+00
11	1.000E+00	5.978E−01	1.976E+00	2.479E+00	2.544E+00	2.403E+00	2.087E+00	1.801E+00	1.502E+00
12	1.585E+00	4.793E−01	1.861E+00	2.461E+00	2.620E+00	2.518E+00	2.225E+00	1.920E+00	1.611E+00
13	2.512E+00	3.827E−01	1.736E+00	2.418E+00	2.665E+00	2.605E+00	2.347E+00	2.026E+00	1.711E+00
14	3.981E+00	3.050E−01	1.609E+00	2.357E+00	2.681E+00	2.669E+00	2.452E+00	2.129E+00	1.806E+00
15	6.310E+00	2.432E−01	1.483E+00	2.282E+00	2.670E+00	2.709E+00	2.538E+00	2.227E+00	1.895E+00
16	1.000E+01	1.941E−01	1.359E+00	2.192E+00	2.635E+00	2.724E+00	2.597E+00	2.309E+00	1.974E+00
17	1.585E+01	1.548E−01	1.237E+00	2.086E+00	2.581E+00	2.714E+00	2.623E+00	2.368E+00	2.038E+00
18	2.512E+01	1.234E−01	1.119E+00	1.971E+00	2.510E+00	2.685E+00	2.625E+00	2.407E+00	2.090E+00
19	3.981E+01	9.832E−02	1.008E+00	1.855E+00	2.424E+00	2.647E+00	2.617E+00	2.431E+00	2.132E+00
20	6.310E+01	7.830E−02	9.048E−01	1.741E+00	2.327E+00	2.602E+00	2.603E+00	2.445E+00	2.166E+00
21	1.000E+02	6.237E−02	8.109E−01	1.628E+00	2.230E+00	2.552E+00	2.587E+00	2.453E+00	2.195E+00
22	1.585E+02	4.965E−02	7.271E−01	1.515E+00	2.139E+00	2.495E+00	2.568E+00	2.459E+00	2.220E+00
23	2.512E+02	3.956E−02	6.515E−01	1.406E+00	2.053E+00	2.436E+00	2.544E+00	2.461E+00	2.243E+00
24	3.981E+02	3.158E−02	5.817E−01	1.306E+00	1.973E+00	2.377E+00	2.511E+00	2.457E+00	2.263E+00
25	6.310E+02	2.528E−02	5.178E−01	1.215E+00	1.893E+00	Z.319E+00	2.470E+00	2.448E+00	2.280E+00
26	1.000E+03	2.031E−02	4.620E−01	1.133E+00	1.806E+00	2.256E+00	2.429E+00	2.435E+00	2.297E+00
27	1.585E+03	1.630E−02	4.145E−01	1.056E+00	1.710E+00	2.185E+00	2.394E+00	2.417E+00	2.311E+00
28	2.512E+03	1.284E−02	3.665E−01	9.860E−01	1.618E+00	2.116E+00	2.360E+00	2.396E+00	2.319E+00
29	3.981E+03	9.972E−03	3.227E−01	9.202E−01	1.533E+00	2.051E+00	2.321E+00	2.374E+00	2.321E+00
30	6.310E+03	7.847E−03	2.896E−01	8.548E−01	1.453E+00	1.987E+00	2.275E+00	2.354E+00	2.322E+00
31	1.000E+04	6.261E−03	2.600E−01	7.896E−01	1.377E+00	1.920E+00	2.227E+00	2.338E+00	2.322E+00
32	1.585E+04	5.029E−03	2.283E−01	7.255E−01	1.306E+00	1.846E+00	2.183E+00	2.330E+00	2.323E+00
33	2.512E+04	4.088E−03	1.981E−01	6.655E−01	1.242E+00	1.775E+00	2.145E+00	2.329E+00	2.325E+00
34	3.981E+04	3.421E−03	1.710E−01	6.083E−01	1.181E+00	1.711E+00	2.112E+00	2.335E+00	2.334E+00
35	6.310E+04	2.987E−03	1.435E−01	5.476E−01	1.105E+00	1.646E+00	2.079E+00	2.342E+00	2.361E+00
36	1.000E+05	2.680E−03	1.176E−01	4.841E−01	1.017E+00	1.570E+00	2.035E+00	2.334E+00	2.402E+00
37	1.585E+05	2.436E−03	9.434E−02	4.172E−01	9.197E−01	1.472E+00	1.969E+00	2.305E+00	2.447E+00
38	2.512E+05	2.270E−03	7.107E−02	3.441E−01	8.115E−01	1.347E+00	1.868E+00	2.254E+00	2.465E+00
39	3.981E+05	2.105E−03	5.030E−02	2.708E−01	6.831E−01	1.198E+00	1.720E+00	2.156E+00	2.423E+00
40	6.310E+05	2.040E−03	3.452E−02	2.018E−01	5.515E−01	1.023E+00	1.524E+00	1.983E+00	2.300E+00
41	1.000E+06	2.134E−03	2.421E−02	1.414E−01	4.288E−01	8.236E−01	1.282E+00	1.724E+00	2.084E+00
42	1.585E+06	2.268E−03	1.635E−02	9.408E−02	3.060E−01	6.146E−01	1.004E+00	1.406E+00	1.777E+00
43	2.512E+06	2.255E−03	1.020E−02	6.011E−02	1.955E−01	4.232E−01	7.265E−01	1.067E+00	1.408E+00
44	3.981E+06	1.959E−03	6.505E−03	3.660E−02	1.193E−01	2.761E−01	4.912E−01	7.482E−01	1.028E+00
45	6.310E+06	1.538E−03	4.031E−03	2.085E−02	6.880E−02	1.671E−01	3.080E−01	4.807E−01	6.825E−01
46	1.000E+07	1.133E−03	2.297E−03	1.151E−02	3.803E−02	9.605E−02	1.827E−01	2.950E−01	4.230E−01
47	1.585E+07	7.677E−04	1.539E−03	7.097E−03	2.439E−02	6.111E−02	1.144E−01	1.891E−01	2.730E−01
48	2.512E+07	6.039E−04	9.713E−04	3.868E−03	1.238E−02	3.130E−02	6.324E−02	1.032E−01	1.603E−01
49	3.000E+07	6.216E−04	8.569E−04	2.978E−03	8.590E−03	2.237E−02	4.309E−02	7.788E−02	1.196E−01

Table 4 continued

Number	E [eV]	5.5 in.	6 in.	6.5 in.	7 in.	7.5 in.	8 in.	8.5 in.	9 in.
1	1.000E−02	2.991E−01	2.393E−01	1.966E−01	1.615E−01	1.259E−01	9.352E−02	7.028E−02	5.494E−02
2	1.585E−02	3.290E−01	2.690E−01	2.213E−01	1.797E−01	1.390E−01	1.045E−01	7.893E−02	6.203E−02
3	2.512E−02	3.701E−01	3.050E−01	2.508E−01	2.025E−01	1.575E−01	1.194E−01	9.132E−02	7.202E−02
4	3.981E−02	4.316E−01	3.534E−01	2.894E−01	2.340E−01	1.849E−01	1.411E−01	1.102E−01	8.703E−02
5	6.310E−02	5.137E−01	4.181E−01	3.401E−01	2.748E−01	2.197E−01	1.699E−01	1.344E−01	1.062E−01
6	1.000E−01	6.151E−01	5.031E−01	4.056E−01	3.250E−01	2.586E−01	2.050E−01	1.620E−01	1.280E−01
7	1.585E−01	7.330E−01	6.088E−01	4.864E−01	3.841E−01	2.994E−01	2.454E−01	1.912E−01	1.511E−01
8	2.512E−01	8.603E−01	7.229E−01	5.747E−01	4.492E−01	3.440E−01	2.879E−01	2.219E−01	1.750E−01
9	3.981E−01	9.888E−01	8.304E−01	6.607E−01	5.171E−01	3.953E−01	3.290E−01	2.541E−01	1.995E−01
10	6.310E−01	1.112E+00	9.251E−01	7.393E−01	5.843E−01	4.529E−01	3.671E−01	2.868E−01	2.240E−01
11	1.000E+00	1.226E+00	1.010E+00	8.100E−01	6.475E−01	5.090E−01	4.024E−01	3.161E−01	2.464E−01
12	1.585E+00	1.329E+00	1.089E+00	8.734E−01	7.042E−01	5.572E−01	4.356E−01	3.394E−01	2.654E−01
13	2.512E+00	1.423E+00	1.165E+00	9.335E−01	7.555E−01	5.988E−01	4.671E−01	3.611E−01	2.835E−01
14	3.981E+00	1.508E+00	1.238E+00	9.952E−01	8.032E−01	6.374E−01	4.976E−01	3.870E−01	3.038E−01
15	6.310E+00	1.587E+00	1.308E+00	1.058E+00	8.481E−01	6.744E−01	5.272E−01	4.168E−01	3.259E−01
16	1.000E+01	1.656E+00	1.370E+00	1.114E+00	8.899E−01	7.091E−01	5.555E−01	4.437E−01	3.463E−01
17	1.585E+01	1.716E+00	1.422E+00	1.161E+00	9.284E−01	7.412E−01	5.822E−01	4.630E−01	3.623E−01
18	2.512E+01	1.768E+00	1.467E+00	1.199E+00	9.637E−01	7.708E−01	6.076E−01	4.788E−01	3.755E−01
19	3.981E+01	1.815E+00	1.508E+00	1.234E+00	9.963E−01	7.982E−01	6.320E−01	4.969E−01	3.887E−01
20	6.310E+01	1.858E+00	1.548E+00	1.268E+00	1.027E+00	8.243E−01	6.559E−01	5.186E−01	4.033E−01
21	1.000E+02	1.895E+00	1.583E+00	1.300E+00	1.056E+00	8.501E−01	6.797E−01	5.406E−01	4.191E−01
22	1.585E+02	1.927E+00	1.615E+00	1.331E+00	1.084E+00	8.764E−01	7.037E−01	5.601E−01	4.360E−01
23	2.512E+02	1.956E+00	1.645E+00	1.362E+00	1.113E+00	9.032E−01	7.280E−01	5.775E−01	4.538E−01
24	3.981E+02	1.985E+00	1.676E+00	1.395E+00	1.141E+00	9.302E−01	7.529E−01	5.937E−01	4.726E−01
25	6.310E+02	2.014E+00	1.709E+00	1.430E+00	1.169E+00	9.574E−01	7.784E−01	6.104E−01	4.922E−01
26	1.000E+03	2.043E+00	1.743E+00	1.465E+00	1.198E+00	9.856E−01	8.046E−01	6.295E−01	5.126E−01
27	1.585E+03	2.071E+00	1.776E+00	1.497E+00	1.229E+00	1.015E+00	8.316E−01	6.529E−01	5.335E−01
28	2.512E+03	2.095E+00	1.806E+00	1.528E+00	1.263E+00	1.047E+00	8.596E−01	6.798E−01	5.549E−01
29	3.981E+03	2.116E+00	1.834E+00	1.560E+00	1.302E+00	1.082E+00	8.887E−01	7.087E−01	5.766E−01
30	6.310E+03	2.134E+00	1.861E+00	1.595E+00	1.346E+00	1.121E+00	9.187E−01	7.381E−01	5.982E−01
31	1.000E+04	2.150E+00	1.892E+00	1.636E+00	1.395E+00	1.162E+00	9.494E−01	7.671E−01	6.196E−01
32	1.585E+04	2.168E+00	1.930E+00	1.686E+00	1.447E+00	1.207E+00	9.813E−01	7.950E−01	6.405E−01
33	2.512E+04	2.187E+00	1.979E+00	1.747E+00	1.502E+00	1.255E+00	1.018E+00	8.210E−01	6.605E−01
34	3.981E+04	2.215E+00	2.042E+00	1.820E+00	1.564E+00	1.312E+00	1.067E+00	8.564E−01	6.903E−01
35	6.310E+04	2.265E+00	2.121E+00	1.909E+00	1.648E+00	1.395E+00	1.144E+00	9.240E−01	7.504E−01
36	1.000E+05	2.347E+00	2.223E+00	2.031E+00	1.784E+00	1.522E+00	1.259E+00	1.028E+00	8.406E−01
37	1.585E+05	2.460E+00	2.362E+00	2.201E+00	1.982E+00	1.703E+00	1.422E+00	1.175E+00	9.666E−01
38	2.512E+05	2.561E+00	2.538E+00	2.412E+00	2.199E+00	1.925E+00	1.637E+00	1.383E+00	1.155E+00
39	3.981E+05	2.596E+00	2.665E+00	2.598E+00	2.417E+00	2.179E+00	1.908E+00	1.660E+00	1.424E+00
40	6.310E+05	2.553E+00	2.704E+00	2.717E+00	2.613E+00	2.441E+00	2.218E+00	1.995E+00	1.771E+00
41	1.000E+06	2.412E+00	2.622E+00	2.721E+00	2.727E+00	2.644E+00	2.503E+00	2.329E+00	2.146E+00
42	1.585E+06	2.125E+00	2.374E+00	2.544E+00	2.634E+00	2.655E+00	2.615E+00	2.523E+00	2.407E+00
43	2.512E+06	1.728E+00	2.001E+00	2.206E+00	2.354E+00	2.461E+00	2.512E+00	2.516E+00	2.488E+00
44	3.981E+06	1.311E+00	1.588E+00	1.787E+00	1.984E+00	2.125E+00	2.225E+00	2.310E+00	2.371E+00
45	6.310E+06	9.054E−01	1.136E+00	1.322E+00	1.509E+00	1.659E+00	1.761E+00	1.871E+00	1.971E+00
46	1.000E+07	5.722E−01	7.284E−01	8.915E−01	1.023E+00	1.163E+00	1.248E+00	1.339E+00	1.431E+00
47	1.585E+07	3.724E−01	4.766E−01	5.798E−01	6.822E−01	7.859E−01	8.785E−01	9.536E−01	1.031E+00
48	2.512E+07	2.239E−01	2.875E−01	3.543E−01	4.228E−01	4.955E−01	5.683E−01	6.252E−01	6.826E−01
49	3.000E+07	1.728E−01	2.307E−01	2.853E−01	3.379E−01	3.923E−01	4.467E−01	4.969E−01	5.447E−01

Table 4 continued

Number	E [eV]	9.5 in.	10 in.	10.5 in.	11 in.	11.5 in.	12 in.	15 in.
1	1.000E−02	4.486E−02	3.735E−02	3.021E−02	2.333E−02	1.711E−02	1.196E−02	2.811E−03
2	1.585E−02	5.071E−02	4.233E−02	3.431E−02	2.683E−02	2.013E−02	1.454E−02	3.302E−03
3	2.512E−02	5.867E−02	4.852E−02	3.932E−02	3.087E−02	2.342E−02	1.725E−02	3.821E−03
4	3.981E−02	7.029E−02	5.688E−02	4.592E−02	3.585E−02	2.721E−02	2.025E−02	4.405E−03
5	6.310E−02	8.488E−02	6.739E−02	5.374E−02	4.163E−02	3.156E−02	2.376E−02	5.140E−03
6	1.000E−01	1.012E−01	7.977E−02	6.222E−02	4.794E−02	3.652E−02	2.803E−02	6.121E−03
7	1.585E−01	1.183E−01	9.364E−02	7.095E−02	5.463E−02	4.211E−02	3.318E−02	7.377E−03
8	2.512E−01	1.360E−01	1.081E−01	8.032E−02	6.200E−02	4.838E−02	3.883E−02	8.674E−03
9	3.981E−01	1.545E−01	1.223E−01	9.093E−02	7.047E−02	5.540E−02	4.449E−02	9.724E−03
10	6.310E−01	1.736E−01	1.358E−01	1.028E−01	8.000E−02	6.297E−02	4.985E−02	1.055E−02
11	1.000E+00	1.916E−01	1.490E−01	1.148E−01	8.959E−02	7.041E−02	5.484E−02	1.146E−02
12	1.585E+00	2.076E−01	1.621E−01	1.260E−01	9.836E−02	7.705E−02	5.939E−02	1.271E−02
13	2.512E+00	2.226E−01	1.748E−01	1.362E−01	1.063E−01	8.272E−02	6.357E−02	1.409E−02
14	3.981E+00	2.384E−01	1.866E−01	1.457E−01	1.137E−01	8.737E−02	6.744E−02	1.535E−02
15	6.310E+00	2.548E−01	1.980E−01	1.547E−01	1.207E−01	9.140E−02	7.119E−02	1.633E−02
16	1.000E+01	2.705E−01	2.098E−01	1.637E−01	1.275E−01	9.568E−02	7.504E−02	1.704E−02
17	1.585E+01	2.841E−01	2.228E−01	1.727E−01	1.344E−01	1.009E−01	7.917E−02	1.754E−02
18	2.512E+01	2.966E−01	2.355E−01	1.815E−01	1.410E−01	1.066E−01	8.344E−02	1.802E−02
19	3.981E+01	3.092E−01	2.465E−01	1.898E−01	1.473E−01	1.123E−01	8.766E−02	1.873E−02
20	6.310E+01	3.222E−01	2.553E−01	1.974E−01	1.532E−01	1.177E−01	9.176E−02	1.966E−02
21	1.000E+02	3.350E−01	2.631E−01	2.046E−01	1.589E−01	1.229E−01	9.578E−02	2.056E−02
22	1.585E+02	3.471E−01	2.710E−01	2.115E−01	1.644E−01	1.279E−01	9.976E−02	2.124E−02
23	2.512E+02	3.586E−01	2.797E−01	2.184E−01	1.698E−01	1.328E−01	1.037E−01	2.185E−02
24	3.981E+02	3.699E−01	2.897E−01	2.253E−01	1.752E−01	1.376E−01	1.075E−01	2.257E−02
25	6.310E+02	3.814E−01	3.006E−01	2.325E−01	1.806E−01	1.421E−01	1.111E−01	2.347E−02
26	1.000E+03	3.936E−01	3.107E−01	2.398E−01	1.861E−01	1.464E−01	1.146E−01	2.443E−02
27	1.585E+03	4.069E−01	3.190E−01	2.476E−01	1.918E−01	1.505E−01	1.178E−01	2.537E−02
28	2.512E+03	4.215E−01	3.274E−01	2.564E−01	1.979E−01	1.545E−01	1.210E−01	2.633E−02
29	3.981E+03	4.376E−01	3.407E−01	2.667E−01	2.050E−01	1.591E−01	1.244E−01	2.734E−02
30	6.310E+03	4.555E−01	3.603E−01	2.793E−01	2.137E−01	1.646E−01	1.284E−01	2.839E−02
31	1.000E+04	4.752E−01	3.810E−01	2.943E−01	2.242E−01	1.718E−01	1.336E−01	2.952E−02
32	1.585E+04	4.975E−01	3.996E−01	3.120E−01	2.371E−01	1.813E−01	1.406E−01	3.075E−02
33	2.512E+04	5.242E−01	4.207E−01	3.332E−01	2.532E−01	1.939E−01	1.496E−01	3.204E−02
34	3.981E+04	5.594E−01	4.496E−01	3.576E−01	2.733E−01	2.100E−01	1.611E−01	3.340E−02
35	6.310E+04	6.108E−01	4.907E−01	3.896E−01	3.016E−01	2.321E−01	1.776E−01	3.585E−02
36	1.000E+05	6.848E−01	5.531E−01	4.403E−01	3.459E−01	2.669E−01	2.052E−01	4.122E−02
37	1.585E+05	7.918E−01	6.455E−01	5.192E−01	4.129E−01	3.219E−01	2.507E−01	5.189E−02
38	2.512E+05	9.578E−01	7.865E−01	6.434E−01	5.185E−01	4.141E−01	3.295E−01	6.964E−02
39	3.981E+05	1.209E+00	1.014E+00	8.534E−01	7.014E−01	5.728E−01	4.651E−01	9.894E−02
40	6.310E+05	1.554E+00	1.345E+00	1.160E+00	9.749E−01	8.122E−01	6.731E−01	1.743E−01
41	1.000E+06	1.950E+00	1.746E+00	1.539E+00	1.330E+00	1.138E+00	9.703E−01	3.390E−01
42	1.585E+06	2.260E+00	2.093E+00	1.909E+00	1.725E+00	1.542E+00	1.373E+00	6.339E−01
43	2.512E+06	2.408E+00	2.312E+00	2.191E+00	2.060E+00	1.922E+00	1.779E+00	1.016E+00
44	3.981E+06	2.354E+00	2.346E+00	2.292E+00	2.194E+00	2.115E+00	2.008E+00	1.365E+00
45	6.310E+06	2.012E+00	2.055E+00	2.063E+00	2.019E+00	1.990E+00	1.930E+00	1.507E+00
46	1.000E+07	1.503E+00	1.553E+00	1.600E+00	1.618E+00	1.625E+00	1.613E+00	1.433E+00
47	1.585E+07	1.083E+00	1.131E+00	1.177E+00	1.216E+00	1.243E+00	1.258E+00	1.255E+00
48	2.512E+07	7.220E−01	7.642E−01	8.044E−01	8.427E−01	8.759E−01	9.016E−01	9.699E−01
49	3.000E+07	5.871E−01	6.295E−01	6.680E−01	7.052E−01	7.389E−01	7.678E−01	8.511E−01

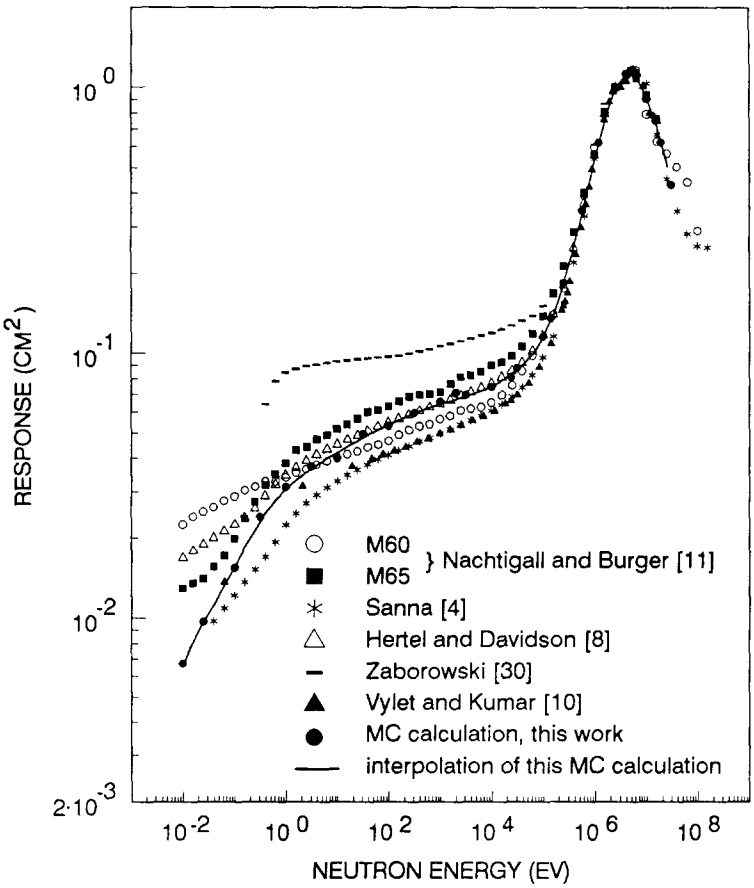

Fig. 9. Comparison of the presently calculated energy response of the 12 in. sphere with data from the literature.

shown. The data are shown together with the final response matrix data for these spheres interpolated in the energy domain. In only 21% of the cases were the differences greater than 1% but none were larger than 5.4%. The fine discrepancies result from MCNP uncertainties and from the double use of the cubic spline interpolation for these spheres not included in Monte Carlo calculations.

The full data of the interpolated response matrix for the BSS with ^{3}He counter are listed in table 4, together with the response of the bare ^{3}He detector.

4.6. Comparison with experimental and other calculated data

A first comparison with recent experimental data [15], which were determined by using partly the same detector system, exhibit good agreement even on an absolute scale.

In order to compare the present calculated response matrix with other well known and frequently used matrices of various BSS systems, all essential response functions available from the literature for the 12 in. sphere are plotted together in fig. 9: the original data of Bramblett et al. [1] and McGuire [2] as interpolated by Nachtigall and Burger [11], for 12.7×12.7 mm ^{6}LiI scintillator [4], for 4×4 mm ^{6}LiI [8,31] and for a 9×9 mm diameter ^{3}He cylindrical counter [10]. The responses were normalised to the value corresponding at an energy of 2.5 MeV which is one of 14 energy points recommended by ISO [20]. This was necessary because of the different sensitivities of the respective thermal neutron detectors. The 12 in. sphere was selected because the thickness of the moderating sphere is large enough to minimise the influence of different detector volumes. Furthermore, its response is similar to the fluence to dose equivalent conversion functions h_{MADE} and $h^*(10)$ [32,33].

From fig. 9 it is evident that response matrices differ in shape. The largest deviations occur with the response matrix based on the hypothesis of Zaborowski [30] as constructed by Alevra and Siebert [31]. The other responses show almost the same general trend over the whole energy scale except for thermal to 1 eV energies, where significant discrepancies are observed.

This effect may be due to the following reasons:

– the poor thermal neutron experimental data [1] on which the interpolation of the matrix referred to as M6O was based;

– the use of different methods to solve the transport equation, i.e. the adjoint transport technique of Hansen and Sandmeier [21] for the M65 matrix, the ANISN code used by Hertel and Davidson [8] and Vylet [10], the code DTF-IV used by Sanna [4] and the MCNP Monte Carlo code used in the present calculation;

– the lower density ($\rho = 0.92$ g cm^{-3}) of polyethylene in Zaborowski's data [30] and in the most recently estimated response matrix for BSS with ^{3}He counter of Vylet [10];

– the different neutron cross section libraries used in the calculations may have introduced differences of response matrices.

A final comparison will only be possible when the final evaluation of the experimental data is available [34]. However, it can be already stated that these experimental data fully support the results presented in this article in the whole energy range, including the above discussed critical interval from thermal to 1 eV.

5. Summary and conclusions

The full data matrix for a Bonner sphere spectrometer based on a 3.2 cm diameter ^{3}He proportional counter for neutrons from thermal to 30 MeV is presented. The calculations with the Monte Carlo code MCNP were performed for sphere diameters down to 2 in., although for this value the moderating shell becomes thin due to the relatively large volume of the proportional counter. Numerical values of responses calculated with MCNP were then used to generate the response matrix having 49 energy points and 21 sphere diameters using the cubic spline interpolation method.

The following observations are made:

1) First estimates show very good agreement with recent experimental data.

2) Deviations from other calculated matrices may be due to lack of cross section data and to improper transport calculation method, but also due to different detector sizes, especially at small sphere diameters, e.g. less than 5 in.

3) The semi-empirical log–normal representation of the responses versus the sphere diameter fits the calculated data well, although for some conditions systematic differences are observed. It may be used to provide good initial estimates.

4) The dependence of the absolute response to the ^{3}He gas pressure is nearly linear and independent of the sphere diameter in the vicinity of the reference pressure (172 kPa).

5) The influence of density of the polyethylene spheres is considerable and should be taken into account when in practice the density can vary a lot.

Acknowledgements

The authors are indebted to Mr. R. Mederer of the Computer Center, GSF for his efficient system support and to Mr. A. Wittmann of the Institut für Strahlenschutz for providing the spline interpolation computer program.

The authors wish to express their thanks to Dr. J. Arkuszewski from Paul-Scherrer-Institut in Würenlingen, Switzerland, for the helpful discussions on the various aspects of MNCP calculations.

The work was partly supported by the Commission of the European Community under contract No. B17-0031-C; this is gratefully acknowledged.

Note

The full data of the Bonner sphere matrix are available on any standard PC-diskette upon request.

References

[1] R.L. Bramblett, R.I. Ewing and T.W. Bonner, Nucl. Instr. and Meth. 9 (1960) 1.
[2] S.A. McGuire, LANL Report LA-3435 (1966).
[3] F. Grünauer and G. Burger, GSF-Report S99 (1970).
[4] R.S. Sanna, Report HASL-267 (1973).
[5] M.P. Dhairyawan, P.S. Nagarajan and G. Venkataraman, Nucl. Instr. and Meth. 169 (1980) 115.
[6] H. Schraube, Proc. 5th Symp. on Neutron Dosimetry, EUR 9762, Vol.1 (1985) p. 583.
[7] M. Awschalom and R.S. Sanna, Radiat. Prot. Dosim. 10 (1985) 89.
[8] N.E. Hertel and J.W. Davidson, Nucl. Instr. and Meth. A238 (1985) 509.
[9] K.A. Lowry and T.L. Johnson, Health Phys. 50 (1986) 543.
[10] V. Vylet and A. Kumar, Nucl. Instr. and Meth. A271 (1988) 607.
[11] D. Nachtigall and G. Burger, in: Topics in Radiation Dosimetry, Suppl. 1 (Academic Press, 1972) p. 385.
[12] J.T. Routti and J.V. Sandberg, Radiat. Prot. Dosim. 10 (1985) 103.
[13] A.V. Alevra, B.R.L. Siebert, A. Aroua, M. Buxerolle, M. Grecescu, M. Katzke, M. Mourges, C.A. Perks, H. Schraube, D.T. Thomas and H.L. Zaborowski, PTB-Report, PTB-7.22-90-1 (1990).
[14] M. Mourgues, Proc. 2nd Symp. on Neutron Dosimetry, EUR 5273, Vol. 2 (1975) p. 907.
[15] A.V. Alevra, M. Cosack, J.B. Hunt, D.T. Thomas and H. Schraube, Radiat. Prot. Dosim. 23 (1988) 293.
[16] H. Schraube, Radiat. Prot. Dosim. 20 (1987) 9.
[17] J.B. Hunt, Radiat. Prot. Dosim. 8 (1984) 239.
[18] H. Schraube, J.L. Chartier, M. Cosack, H.J. Delafield, J.B. Hunt and R.B. Schwartz, Radiat. Prot. Dosim. 23 (1988) 217.
[19] D.J. Thomas and N. Soochak, NPL Report RS 104 (1988).

[20] International Standard, Geneve, ISO 8529 (1989).
[21] G.E. Hansen and H.A. Sandmeier, Nucl. Sci. Eng. 22 (1965) 315.
[22] W.W. Engle, ORNL Report K-1693, Oak Ridge (1967).
[23] H. Lichtenstein, M.O. Cohen, H.A. Steinberg, E.S. Treubetzkoy and M. Beer, Computer code manual CCM-8, MAGI, New York (1979).
[24] J.F. Briesmeister (ed.), Report LA-7396-K, Rev. 2, Los Alamos (1986).
[25] N.S. Cramer, Report ORNL/TM-9641 (1985).
[26] R.E. MacFarlane et al., Report LA-9303-M, (ENDF-324), Los Alamos (1982).
[27] D. Garber (ed.), Report BNL-17541, (ENDF-201), Upton, NY (1975).
[28] R.J. Howerton, D.E. Cutter, R.C. Haight, M.H. MacGregor, S.T. Perkins and E.F. Plechaty, LLNL Report UCRL-50400 (1975).
[29] J.U. Koppel and D.H. Houston, Report GA-8744 (1978).
[30] H.L. Zaborowski, Proc. 4th Symp. on Neutron Dosimetry, EUR 7448 (1981) 575.
[31] A.Y. Alevra and B.R.L. Siebert, PTB Report PTB-ND-28 (1986).
[32] ICRP-Report 21 (Pergamon, 1978).
[33] ICRU-Report 43, Int. Comm. Rad. Units Meas., Bethesda (1988).
[34] A.Y. Alevra, M. Cosack, J.B. Hunt, D.J. Thomas and H. Schraube, to be published in Radiat. Prot. Dosim. (1991).